

OFFSET HEIGHT EFFECTS ON TURBULENT CHARACTERISTICS OF SUBMERGED JETS

Mohammad S. Rahman

Department of Mechanical Engineering
University of Manitoba
Winnipeg, Manitoba, Canada
rahmanms@myumanitoba.ca

Godwin F.K. Tay

Department of Mechanical Engineering
University of Manitoba
Winnipeg, Manitoba, Canada
kwakutay@gmail.com

Mark F. Tachie

Department of Mechanical Engineering
University of Manitoba
Winnipeg, Manitoba, Canada
mark.tachie@umanitoba.ca

ABSTRACT

Experimental study of turbulent characteristics of submerged jet near the free surface was carried out at four offset height ratios of 1, 2, 3 and 4. The Reynolds number based on jet exit velocity and nozzle width was 5500. A particle image velocimetry system was used for the velocity measurement. The jet attachment length increased with the offset height. The results showed that the free surface affected the maximum velocity decay and jet spread for the shallower jets. The surface mean velocity and Reynolds normal stresses were quantified and dramatic reduction of surface-normal Reynolds normal stress than its streamwise component was observed in the interaction region. Joint probability density functions were used to investigate the contribution of the turbulent events to Reynolds shear stress.

INTRODUCTION

Turbulent jets discharged in the vicinity of a free surface are often referred to as submerged jets. Submerged jets have various practical applications which include disposal of industrial effluent into shallow streams, water purification, and in the remote sensing of moving ships. Understanding the mixing characteristics and turbulent structures in submerged jets is important to the design of engineering devices.

A schematic diagram of a submerged jet is shown in figure 1. The nozzle of width, d is located near the free surface. The offset height of the center of the nozzle from the free surface is denoted by h . The origin of the Cartesian coordinate system adopted in the present study is located at the center of the nozzle in the jet exit plane; x and y indicate the streamwise and surface-normal direction respectively, U and V indicate the streamwise and surface-normal mean velocities respectively, u and v are the streamwise and surface-normal fluctuating velocities respectively; and U_j is the jet exit velocity. The jet attaches to the free surface upon discharge at the attachment point, x_r . The flow field of a submerged jet can be divided into two regions: recirculation region and surface jet region. In the recirculation region, characteristic negative U is found between the upper edge of the jet and the free surface. The streamwise extent of the recirculation region is measured from the nozzle exit to the attachment point and is often referred to as

attachment length. After the recirculation region, surface jet region starts. In the surface jet region, positive U appears at the free surface. One of the salient characteristics of a submerged jet is that the location of local maximum streamwise mean velocity, U_m deviates from the nozzle centerline with the jet development downstream and moves towards the free surface (Anthony and Willmarth, 1992). The dashed line passing through the location of U_m as shown in the figure demarcates the two shear layers of the jet. The upper and lower portion of this dashed line is referred to as upper and lower shear layer, respectively. $y_{0.5}$ and $y^{*0.5}$ are the distances of the location of $0.5U_m$ measured from the location of U_m and the free surface, respectively in the lower shear layer.

The mixing characteristics and turbulent structure of free jets have been extensively investigated in the past (e.g., Gutmark et al. 1989; Hussein et al., 1994; Quinn and Militzer, 1988). It is now widely accepted that the entrainment and spreading characteristics of non-circular jets are considerably different from those in a circular nozzle, due largely to the dynamics of coherent structures. Square jets, for instance, have been found to entrain more fluid and spread more rapidly than their circular counterparts because the vortex rings from rectangular nozzles deform more rapidly and to a greater extent than those in circular nozzles (e.g., Gutmark et al. 1989).

Although the impact of the turbulent structures on the characteristics of free jets is well documented, much less is known concerning the structure of submerged turbulent jets. The interaction between the vortical structures and the free surface was examined by Anthony and Willmarth (1992) for a submerged round jet placed at depth of $h/d = 2$. They reported a redistribution of the turbulent kinetic energy from the surface-normal turbulence intensity to the streamwise and spanwise turbulence intensities. Madnia and Bernal (1994) measured the flow characteristics of an axisymmetric jet issuing at various depths ($h/d = 1, 1.5, 2.5$ and 3.5) beneath and parallel to a free surface. They proposed a model of the free surface as a symmetry plane with the submerged jet interacting with its twin or image jet above the free surface, and h and $U_j d/h$ as the length and velocity scales, respectively, in the surface jet region. Most of the previous studies on submerged turbulent jets used circular nozzles (Madnia and Bernal, 1994; Rainford, and Khan, 2009; Tian et al., 2012; Wallker, et al., 1995).

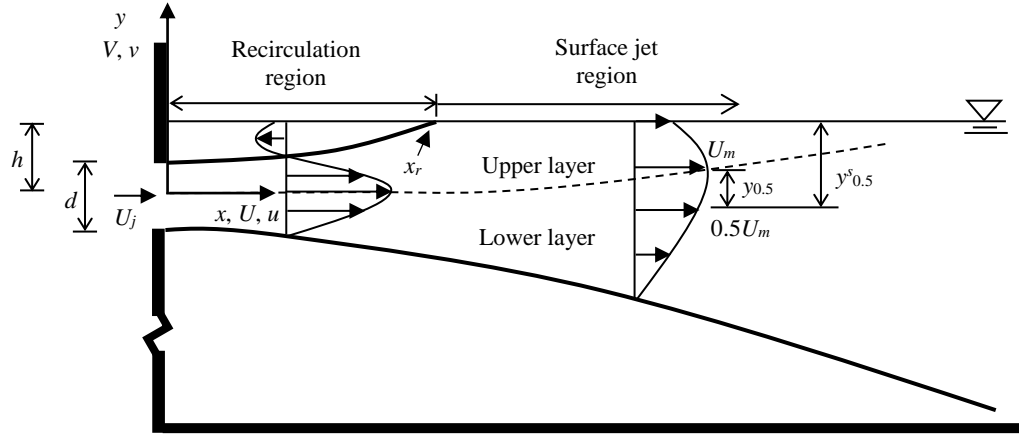


Figure 1. Schematic diagram of submerged jet.

The objective of the present study is to investigate the effects of offset height ratio on the mixing characteristics and turbulent structures in a submerged square jet using a particle image velocimetry system.

EXPERIMENTAL PROCEDURE

The experiments were carried out in an open water channel of length 2500 mm. The cross section of the channel was of dimensions 200 mm \times 200 mm. The channel was fabricated from clear acrylic plates that provide easy optical access. A square orifice nozzle of width, $d = 10$ mm, was used to produce the jet. The following four offset height ratios were tested: $h/d = 1, 2, 3$ and 4. The Reynolds number (Re) and Froude number (Fr) based on U_j and d were approximately 5500 and 1.7, respectively.

A high-resolution particle image velocimetry (PIV) was used to perform the velocity measurements in the vertical symmetry (x - y) plane of the jet. The flow was seeded using 10 μ m silver coated hollow glass spheres with specific gravity of 1.1. The seeding particles were illuminated by a 120 mJ per pulse Nd:YAG double-pulsed laser with a wavelength of 532 nm. A 2048 \times 2048 pixel CCD camera with pixel pitch of 7.4 μ m was used to capture the flow field. The field of view was set to 135 mm \times 135 mm. Measurements were carried out in two planes which cover the streamwise extent of the flow field ranging $0 \leq x/d \leq 24$. Based on an initial convergence test, 5000 image pairs were used to compute the flow statistics. The data were post-processed using the adaptive correlation option of DynamicStudio to obtain the average particle displacement within the interrogation area. The interrogation area size was set as 32 pixels \times 32 pixels with 50% overlap in both x and y directions.

RESULTS AND DISCUSSION

Instantaneous Flow Visualization

Figure 2 shows instantaneous velocity vector field for two offset height cases: $h/d = 1$ and 3 from the jet exit to $x/d = 12$ which covers recirculation region and a portion of surface jet region. A Galilean decomposition was performed by subtracting a constant

convective velocity of $0.15U_j$ from the instantaneous realizations to reveal small scale vortices propagating at that velocity (Agrawal and Prasad, 2002). The corrugated contour lines of $(U - 0.15U_j)$ are also included in the plots to demarcate the turbulent/non-turbulent interface (T/NTI) in the realizations. The contour lines also pass through the centers of the small scale spanwise vortex cores at the edge of the shear layer. Braid-like structures indicated by the darker areas (within $0 < x/d < 7$) are also noticed in the plots, which in the vertical symmetry plane, correspond to the vortex rings propagating in the downstream direction. The results presented in figure 2a provide a clear indication that the jet-free surface interaction limits the T/NTI for the shallower jet in the upper shear layer.

Attachment Length

The attachment length (L_r), measured from the jet exit to the attachment point (x_r) is an important characteristic of submerged jets. In the present study, the attachment point was identified as the streamwise location where the streamwise mean velocity profile along the free surface changes from negative to positive value or starts to increase from a nominally zero value. The estimated values of attachment length were $L_r/d = 1.0, 6.4, 9.3$ and 12.3 for $h/d = 1, 2, 3$ and 4, respectively. The values are about 14 to 20% higher than those reported by Sankar et al. (2008) for a submerged square jet at $Re = 40000$.

Maximum Velocity Decay and Jet Spread

The evolution of the local maximum mean streamwise velocity, U_m as a function of x is shown in figure 3a for the four offset heights. Classical scaling U_j and d are used as the velocity and length scale, respectively, for normalization. U_m decayed with downstream distance due to the entrainment and mixing of the surrounding fluid with the core jet. The decay rate was estimated by fitting a straight line: $U_j/U_m = K_d(x/d - c_1)$ in the linear portion of the U_m profiles as shown in the figure for $h/d = 1$, where K_d and c_1 represent the decay rate and the kinematic virtual origin, respectively. K_d was estimated as 0.149, 0.176, 0.213 and 0.217 for $h/d = 1, 2, 3$ and 4, respectively. The increase in the decay rate with the offset height ratio was due to the enhanced entrainment

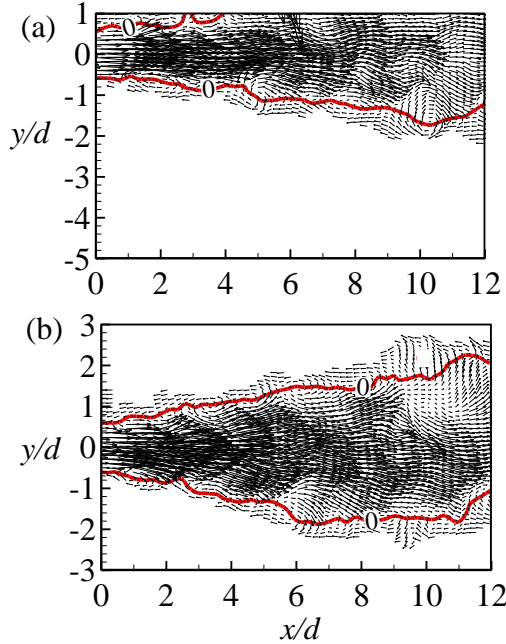


Figure 2. Instantaneous velocity vectors for (a) $h/d = 1$ and (b) $h/d = 3$.

from both the upper and lower side of the jet. The U_m profiles normalized by the similarity variables, h and $U_j d/h$, proposed by Madnia and Bernal (1994) are shown in figure 3b. The profiles for $h/d \geq 2$ collapse reasonably well. A straight line is fitted to the similarity profiles of U_m as shown for $h/d = 1$ in figure 3b and the slope was estimated as 0.149 for $h/d = 1$ and 0.185 for $h/d \geq 2$. The lower value of the slope for $h/d = 1$ indicates a stronger jet-free surface interaction compared to the higher offset height ratio cases. According to the image jet model of Madnia and Bernal (1994), the U_m profile follows the straight line: $(U_j d)/(U_m h) = (K_f/\sqrt{2})(x/d - c_2)$ where K_f and c_2 are the decay rate of a free jet and kinematic virtual origin, respectively. Assuming $K_f = 0.217$, the decay rate for the deepest offset height case ($h/d = 4$), the value $0.217/\sqrt{2} \approx 0.153$ is in reasonable agreement with 0.149 which is the slope obtained from the similarity profiles of U_m for the shallowest case ($h/d = 1$).

The jet spread is characterized by the half velocity width ($y_{0.5}$), the distance between the location of U_m and $0.5U_m$ in the lower shear layer. The variation of $y_{0.5}$ with respect to x/d is shown in figure 4a. The spread rate is quantified by fitting the straight line: $y_{0.5}/d = K_s(x/d - c_3)$ as shown in the figure, where K_s and c_3 represent the spread rate and the geometric virtual origin, respectively. K_s was estimated as 0.085 for $h/d \geq 2$ within $5 \leq x/d \leq 23$. This value of K_s is comparable to the result reported by Quinn and Militzer (1988) and Obot et al. (1984) for free jet. For $h/d = 1$, the spread rate (0.085) was similar to other offset height cases within $x/d \leq 18$. After this point, the value of K_s was decreased to 0.049. The decrease of spread rate for the shallowest case ($h/d = 1$) at larger downstream distance could be attributed to the close proximity of the jet to the free surface which inhibits the entrainment from the upper side of the jet leading to a reduction in the spread rate. The half velocity width measured from the free surface, $y_{0.5}$ following the approach reported by Madnia and

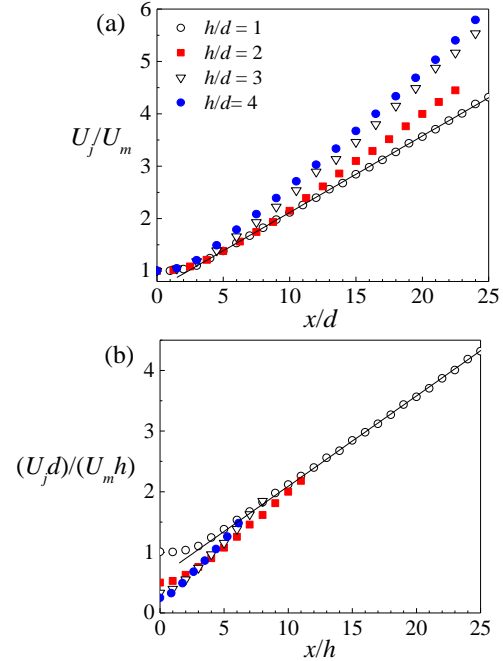


Figure 3. Maximum velocity decay with (a) classical scaling and (b) similarity variables.

Bernal (1994) is estimated and the variation of $y_{0.5}$ with respect to x/h is shown in figure 4b. For $x/h < 13$, $y_{0.5}$ profile for $h/d = 1$ showed a linear distribution with about 17% larger values compared to the higher offset height cases ($h/d \geq 2$). The spread rate was quantified by fitting straight line as shown in the figure where the slope represents the spread rate. The spread rate was estimated as 0.075 irrespective of offset height ratio for $x/h < 13$. Madnia and Bernal (1994) reported a similar spread rate (0.078) within $x/h < 24$ using this scaling. The spread rate for $h/d = 1$ was reduced to 0.055 at $x/h > 13$ which is consistent with the confinement effect discussed earlier in figure 4a.

Profiles of Streamwise Mean Velocity and Reynolds Shear Stress

One dimensional profiles of streamwise mean velocity and Reynolds shear stress at $x/d = 5, 10$ and 20 for $h/d = 1$, the smallest offset height ratio and $h/d = 3$ as a representative of higher offset height ratio are shown in figure 5. The free surface is located at $y/d = 1$ and 3 for $h/d = 1$ and 3 , respectively. The dashed horizontal line in the figure passes through the center of the nozzle. Figure 5a shows that, for $h/d = 1$, positive U appeared at the free surface (at $y/d = 1$) at all of the selected x/d locations as these locations are in the region where jet interacts with the free surface. For $h/d = 3$, U profile at $x/d = 5$, which is upstream of the attachment point ($x/d = 9.3$), is identically zero at the free surface (at $y/d = 3$), however, positive U values were observed at the free surface after the attachment point, i.e., at $x/d = 10$ and 20 .

The profiles of Reynolds shear stress, $-\langle uv \rangle$ are shown in figure 5b. For $h/d = 1$, the peak value of $-\langle uv \rangle$ in the upper shear layer is significantly reduced than in the lower shear layer. The level of reduction in peak value increased with streamwise distance

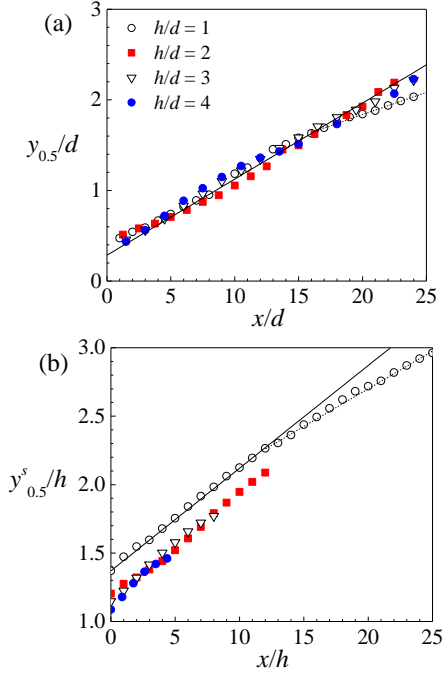


Figure 4. Half velocity width (a) measured from the jet centerline and (b) measured from the free surface.

due to the free surface confinement. This damping of Reynolds shear stress by the free surface reduced with the increase of offset height as observed for $h/d = 3$ case.

Surface Velocity and Reynolds Normal Stresses

The profiles of mean streamwise surface velocity, U_s and surface velocity defect, $\Delta U = U_m - U_s$ for the four offset height ratios are shown in figure 6. Figure 6a shows that U_s was negligibly small from the jet exit to the attachment point. Downstream of the attachment point, the surface flow accelerated to its maximum value. For $h/d = 1$, the maximum value was reached at $x/d \approx 10$. The surface flow is considered to be in a state of strain due to the alternating acceleration ($\partial U_s/\partial x > 0$) and deceleration ($\partial U_s/\partial x < 0$) in the absence of mean surface deformation, and this effect was more dramatic at a shallower offset height. Figure 6b shows the surface velocity profiles normalized by the similarity variables (h and $U_j d/h$) proposed by Madnia and Bernal (1994). The x axis represented as $(x-x_r)$ makes the origin at the attachment point. The similarity scaling shows collapse of the profiles within a limited streamwise distance, $(x-x_r)/h < 4$. Figure 6c shows profiles of the mean surface velocity defect, ΔU normalized by U_m . The profiles showed a good collapse for the chosen velocity scale and follow the following exponential distribution indicated in the figure by the solid line: $U_m/\Delta U = 1 + 0.13 \exp[(x^*)^{0.51}]$, where $x^* = (x-x_r)/h$.

Figure 7a and 7b show the streamwise and surface-normal Reynolds normal stress, $\langle u_s^2 \rangle$ and $\langle v_s^2 \rangle$ normalized by U_j^2 , respectively, along the free surface. The profiles increased rapidly from the relatively low and undisturbed values upstream of the attachment point to their respective peak values. The turbulence levels are relatively higher at a shallower offset height due to the more severe jet-free surface interaction for a shallower jet. After

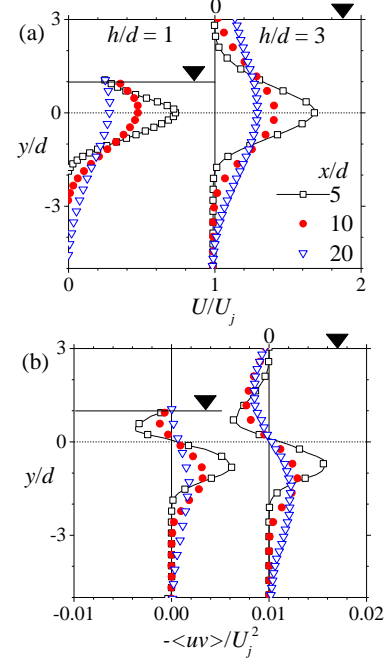


Figure 5. Vertical profiles of (a) streamwise mean velocity and (b) Reynolds shear stress.

reaching to the peak value, the profiles decay, and it is observed that $\langle v_s^2 \rangle$ decayed more rapidly than $\langle u_s^2 \rangle$, which is partly explained by redistribution of turbulent kinetic energy at the free surface from the surface-normal component to the components parallel to the free surface (Anthony and Willmarth, 1992). Figure 7c shows $\langle u_s^2 \rangle$ profiles normalized by $(\Delta U)^2$. A logarithmic scale is used on the vertical axis to show the data for various test cases distinctly. $\langle u_s^2 \rangle$ profiles showed good collapse at higher offset height cases, $h/d \geq 3$ and followed the exponential distribution as shown in the figure by the solid line: $\langle u_s^2 \rangle / (\Delta U)^2 = 0.0045 \exp[(x^*)^{0.9}]$. $\langle v_s^2 \rangle$ profiles (shown as inset) exhibited a similar trend except that the values are relatively lower than $\langle u_s^2 \rangle$, and followed the following exponential distribution for $h/d \geq 3$: $\langle v_s^2 \rangle / (\Delta U)^2 = 0.0018 \exp[(x^*)^{0.8}]$.

Joint Probability Density Functions

The joint probability density function (JPDF) of u and v is used to investigate the effects of the free surface on the contribution of velocity fluctuations to Reynolds shear stress. The JPDFs were estimated using 100×100 bins matrices of velocity fluctuations. Figure 8(a-c) shows JPDF contours at various surface-normal locations for $h/d = 3$ at $x/d = 15$, representing a downstream location where jet-free surface interaction occurs. The selected surface-normal locations are $y^s/d = 1, 3$ and 5 representing a location in the upper shear layer, a location at the jet centerline and a location in the lower shear layer, respectively. Here, y^s is the surface-normal distance measured from the free surface. The axes divide the plots into four quadrants: Q1, Q2, Q3 and Q4 in the u - v parameter plane representing the event of fast entrainment, slow entrainment, slow ejection and fast ejections, respectively. Contour levels of the JPDFs shown in figure 8(a-c) vary from 0.5 to 2.5 at

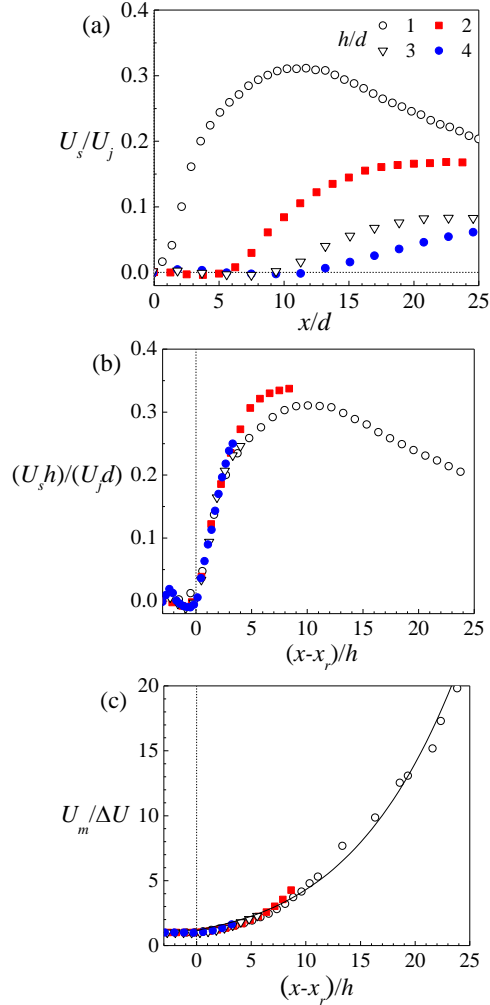


Figure 6. Surface profiles of mean velocity with (a) classical scaling, (b) similarity variables and (c) profiles of velocity defect.

intervals of 0.5. The contours are elliptic in shape and the skewness of the contours towards Q2 and Q4 events at $y^s/d = 1$ (figure 8a) indicated that slow entrainment and fast ejections were the dominant contributors to the Reynolds shear stress in the upper shear layer. On the contrary, the skewness towards Q1 and Q3 events at $y^s/d = 5$ (figures 8c) indicated that fast entrainment and slow ejection were the dominant events in the lower shear layer. It was observed from the JPDF contours (not shown herein) at several surface normal locations in both upper and lower shear layer that away from the jet centerline and as the free surface is approached the contour sizes became smaller due to the reduction in the mean Reynolds shear stress. The angle of inclination of the major axis of the JPDF contours with respect to the streamwise direction was estimated as about 22° in the lower shear layer. This inclination angle in the upper shear layer was about 12% higher than in the lower shear layer indicating free surface effects on the coherent structures in the shear layer. No preferred orientation of the contour to the quadrants was observed at the jet centerline, $y^s/d = 3$ (figure 8b) indicating that the structures were associated equally with the four quadrant events.

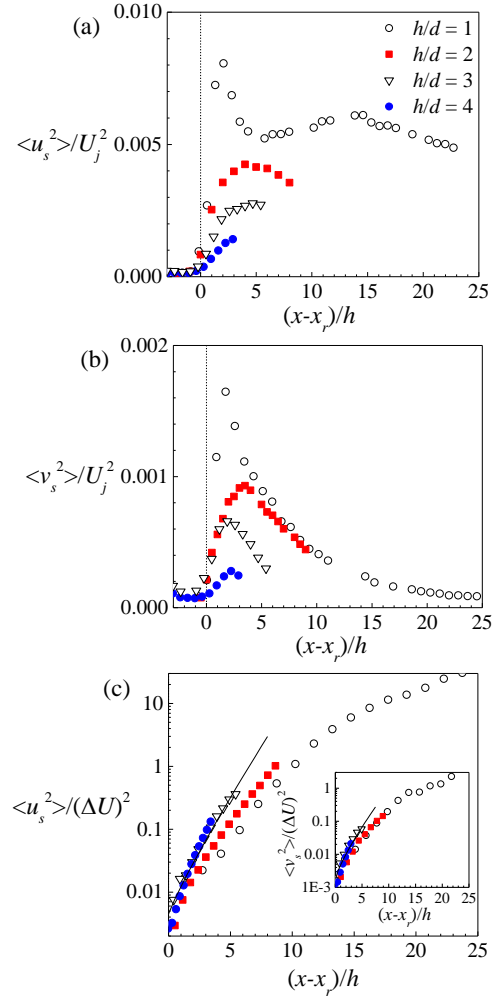


Figure 7. Surface profiles of (a) streamwise Reynolds normal stress and (b) surface-normal Reynolds normal stress normalized by U_j^2 ; and (c) surface profiles of Reynolds normal stresses normalized by $(\Delta U)^2$.

Figures 8(d-f) show the contours of weighted JPDF (WJPDF) where the strength of the correlation between the velocity fluctuations is more evident. Contour levels of the WJPDFs vary from -0.0016 to 0.0016 at intervals of 0.0004. At $y^s/d = 1$ (figure 8d), the positive distribution of WJPDF was larger than the negative distribution which is consistent with the dominance of Q2 and Q4 events in the upper shear layer. At $y^s/d = 5$ (figure 8f), the negative distribution of WJPDF in Q1 and Q3 events was larger than the positive WJPDFs which is in agreement with the JPDF result in the lower shear layer. The WJPDF contours (not shown herein) at several surface-normal locations within the shear layers showed the same damping effect away from the jet center line. WJPDFs in the jet centerline, $y^s/d = 3$ (figure 8e) showed almost similar positive and negative distribution in all four quadrants which supports the equal contribution of all four quadrant events at this location.

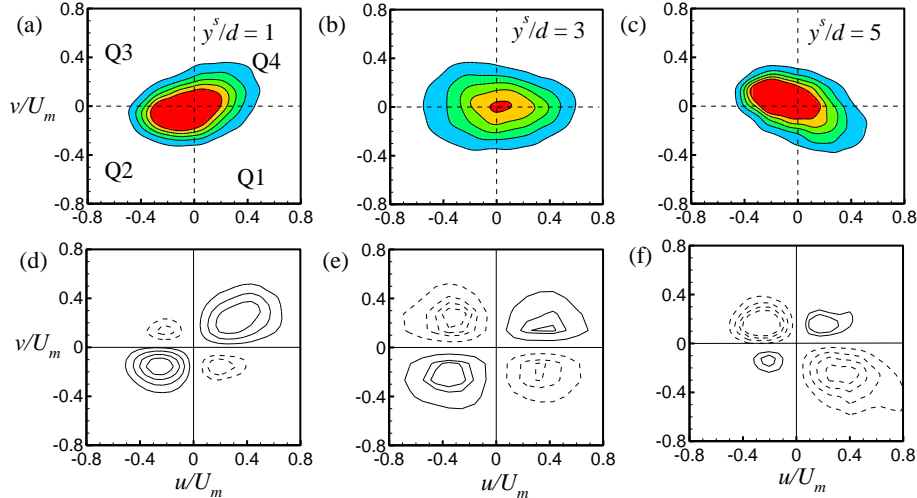


Figure 8. JPDF at (a) $y^s/d = 1$, (b) $y^s/d = 3$ and (c) $y^s/d = 5$; and WJPDF at (d) $y^s/d = 1$, (e) $y^s/d = 3$ and (f) $y^s/d = 5$ at the streamwise location $x/d = 15$ for $h/d = 3$.

CONCLUSION

Turbulent characteristics of submerged square jet were studied experimentally at four offset height ratios, $h/d = 1, 2, 3$ and 4 . The Reynolds number and Froude number based on U_j and d were 5500 and 1.7 , respectively. The instantaneous flow visualization revealed that the free surface diminished the T/NTI for the shallower jet. The attachment length increased from $1.0d$ to $12.3d$ with the increase of offset height ratio from $h/d = 1$ to 4 . The velocity decay rate increased with offset height from $h/d = 1$ to 4 by about 32% due to enhanced entrainment and mixing. The spread rate (0.085) was nearly independent of offset height within $5 \leq x/d \leq 18$. Further downstream, however, the spread rate for the smallest offset height ratio ($h/d = 1$) decreased by about 42% due to the jet's close proximity to the free surface which in turn constrained entrainment of the ambient fluid leading to the reduced spread rate.

The level of Reynolds shear stress is reduced near the free surface and this effect reduced with increasing offset height ratio. The surface velocity profile showed alternating acceleration and deceleration of the surface current and this effect was more intense for the shallower jet. The surface velocity defect (ΔU) profiles collapsed reasonably well and followed an exponential distribution.

The JPDF and WJPDF contours revealed the contribution of the slow entrainment and fast ejection events to the Reynolds shear stress in the upper shear layer; and the contribution of the fast entrainment and slow ejection events in the lower shear layer. The damping effect of the JPDF and WJPDF was observed as the free surface approached due to the reduction in the mean Reynolds shear stress.

ACKNOWLEDGEMENTS

The authors gratefully acknowledge the support of this work by research grants from the Natural Sciences and Engineering Research Council of Canada.

REFERENCES

- Agrawal, A., and Prasad, A. K., 2002, "Properties of vortices in the self-similar turbulent jet," *Experiments in Fluids*, Vol. 33, pp. 565-577.
- Anthony, D. G., and Willmarth, W. W., 1992, "Turbulence measurements in a round jet beneath a free surface," *J. Fluid Mech.*, Vol. 243, pp. 699-720.
- Gutmark, E., Schadow, K. C., Parr, T. P., Hanson-Parr, D. M., and Wilson, K. J., 1989, "Non-circular jets in combustion systems", *Exp. Fluids*, Vol. 7, pp. 248-258.
- Hussein, H. J., Capps, S. P., and George, W. K., 1994, "Velocity measurements in a high-Reynolds-number, momentum-conserving, axisymmetric, turbulent jet," *J. Fluids Mech.*, Vol. 258, pp. 31-75.
- Madnia, C. K., and Bernal, L. P., 1994, "Interaction of a turbulent round jet with the free surface," *J. Fluid Mech.*, Vol. 261, pp. 305-332.
- Obot, N. T., Graska, M. L., and Trabold, T. A., 1984, "The near field behaviour of round jets at moderate Reynolds numbers," *Canad. J. Chem. Engrg.*, Vol. 62, pp. 587-593.
- Quinn, W. R., and Militzer, J., 1988, "Experimental and numerical study of a turbulent free square jet," *Phys. Fluids*, Vol. 31(5), pp. 1017-1025.
- Rainford, J. P., and Khan, A. A., 2009, "Investigation of circular jets in shallow water", *Journal of Hydraulic Research*, Vol. 47(5), pp. 611-618.
- Sankar, G., Balachandar, R., and Carriveau, R., 2008, "Tailwater effects on the characteristics of a square jet near a free-surface," *Journal of Hydraulic Research*, Vol. 46(4), pp. 504-515.
- Tian, J., Roussinova, V., and Balachandar, R., 2012, "Characteristics of a jet in the vicinity of a free surface," *Journal of Fluids Engineering*, Vol. 134, pp. 1-12.
- Walker, D. T., Chen, C. -Y., and Willmarth, W. W., 1995, "Turbulent structure in free-surface jet flows", *J. Fluid Mech.*, Vol. 291, pp. 223-261.